Engineering Applications of Computational Fluid Mechanics Vol. 3, No. 2, pp. 164–174 (2009)

PATTERN COMPETITION IN HOMOGENEOUSLY HEATED FLUID LAYERS

G. M. Cartland Glover*+ and S. C. Generalis**

** Institute of Safety Research, Forschungszentrum Dresden-Rossendorf, POB 51 01 19,*
01314 Dresden, Germany
+ *E-Mail: g.glover@fzd.de* (*Corresponding Author*)
*** School of Engineering and Applied Science, Aston University, Aston Triangle, Birmingham,*
B4 7ET, United Kingdom

ABSTRACT: Simulations examining pattern competition have been performed on a horizontal homogeneously heated layer that is bounded by an isothermal plane above an adiabatic plane. Several different circulation patterns arose as the heating regime applied to the horizontal layer was modified. The sequence of the patterns formed as the Grashof number was increased had the following order: laminar layer, rolls, squares, hexagons and pentagons, and then two square modes of differing orientations. Fourier analysis was used to determine how the key modes interact with each pattern.

Keywords: convection, horizontal layer, heat transfer, stability

---

1. INTRODUCTION

This work is concerned with convection generated by uniformly distributed internal heat sources. The study here is motivated partially by previous work (Busse, 1967; Generalis and Nagata, 2003), but primarily by the fact that the present problem has many important environmental and industrial applications. An industrial example is the case where such convection is driven by a homogeneous heat source that may be produced from fission product decay in a pool of molten fuel elements found at the lower head of a nuclear reactor that is undergoing a severe core damage accident (Asfia and Dhir, 1996). Internal heating also arises in connection with the study of convection in the earth's mantle, where flows are driven by density differences arising from heat generated by the radioactive decay of the elements in the Earth's mantle (Houseman, 1988; Schmalzl, Houseman and Hansen, 1995; Schubert, Glatzmaier and Travis, 1993). Other examples of such convection processes include convective flows arising from biochemical and chemical reactions or from the application of electric currents in conducting fluids (Roberts, 1967; Tritton and Zarraga, 1967). Other numerical studies of natural convection driven by internal heating include the work of Gershuni, Zhukhovitsky and Yakimov (1974), Tveitereid and Palm (1976) and Ichikawa et al. (2006). To numerically resolve the circulation cells of the internally heated layers, Roberts (1967) applied mean-field approximations, while Generalis and Nagata (2003), Gershuni, Zhukhovitsky and Yakimov (1974), Houseman (1988), Schmalzl, Houseman and Hansen (1995), Schubert, Glatzmaier and Travis (1993) and Tveitereid and Palm (1976) all used finite amplitude expansions in the form of pseudospectral codes and Ichikawa et al. (2006) recently implemented a finite volume technique. In addition to these applications, the present problem can be compared with Bénard convection, where motions are driven by temperature differences across the fluid layer and not by homogeneous heating. Useful conclusions can be drawn from such comparisons, but these will be reported elsewhere.

The present study focuses on the numerical simulation of the early stage transition regime of an internally heated convective flow. In this case, the preferred motion of the fluid can be followed when qualitative changes to the fluid motion take place from the mathematically interesting to the more realistic cases. To help understand the formation of the flow patterns that are generated, simulations have been performed on a horizontal layer with Prandtl number 7. The structures of interest are stationary hexagons, squares and rolls, which form at the transition from a laminar convection layer to turbulent convective circulation cells. Stationary circulation cells are stable for a short range of Grashof number after which the flow becomes unstable indicating that the flow patterns are physically realizable only for a small range of the relevant control parameters.

Received: 26 May 2008; Revised: 2 Oct. 2008; Accepted: 9 Oct. 2008

In the following section we present the numerical models employed here. We introduce the relevant boundary conditions and discuss the convergence criteria applied. In section 3 we discuss our results paying particular emphasis on the Fourier and wavenumber analysis of the present study. Finally we make our concluding remarks summarizing the main results of this work.

2. NUMERICAL MODELS

2.1 Governing equations

The flow was resolved by the incompressible form of the conservation equations of (1) mass, (2) momentum and (3) thermal energy using the solver, ANSYS CFX (ANSYS, 2007), where an earlier form of the solver successfully modelled convection rolls in an isothermally bounded cavity (Arter, Bernoff and Newell, 1987);

$$\nabla \cdot \vec{u} = 0 \tag{1}$$

$$\rho_r \frac{\partial \vec{u}}{\partial t} + \rho_r \nabla \cdot \left(\vec{u} \otimes \vec{u} \right) = -\nabla p + \mu \left[\nabla \cdot \vec{u} + \left(\nabla \cdot \vec{u} \right)^T \right] - \vec{g} \rho_r \beta \left(T - T_r \right) + \vec{S} \tag{2}$$

$$\rho_r \frac{\partial e}{\partial t} + \rho_r \nabla \cdot \left(\vec{u} e \right) = - \rho_r k \nabla T + \dot{S} \tag{3}$$

where e, p, T, t and $\vec{u}$ are the internal energy, pressure, temperature, time and the fluid velocity vector. The fluid properties are defined by the specific heat capacity at constant pressure, c_P, thermal conductivity, k, dynamic viscosity, μ and the density, ρ. The terms $\vec{S}$ and $\dot{S}$ introduce the momentum and energy source terms into the respective transport equations. β is the expansion coefficient and $\vec{g}$ is the acceleration due to gravity.

2.2 Boundary conditions

A rectangular layer that has an aspect ratio of $[1:4\sqrt{3}:12]$ was defined according to Ichikawa et al. (2006) where the respective resolution $[30:104:180]$ was used to simulate the cellular convective flow of an incompressible fluid (Fig. 1).

The boundary conditions applied to the planes above and below the internally heated layer were an isothermal plane ($T = T_r$) above an adiabatic plane ($\frac{\partial T}{\partial x} = 0$). The remaining boundaries between the planes are defined as periodic conditions in order to treat the planes as two infinitely sized boundaries.

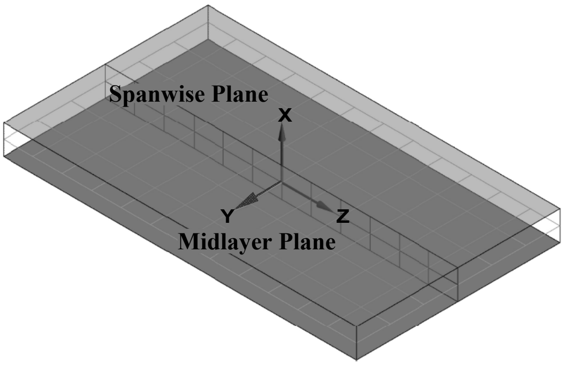

Fig. 1 Diagram of the homogeneous layer with an isothermal surface above an adiabatic surface. The coordinate axis at the origin and the midlayer and spanwise planes are also indicated.

2.3 Non-dimensional parameters

The Grashof number, $Gr = \vec{g}\beta\dot{S}_i L^5 / 2\nu^2 k$, was used to control the value of internal heat source applied to the horizontal layer. Here $\dot{S}_i$ and L are the internal heat source and the width of the layer, whilst $\nu = \mu / \rho$ is the kinematic viscosity and $\alpha = k / c_p \mu$ is the thermal diffusivity. Note that $\dot{S}_i$ was estimated by assuming a temperature difference across the layer and then the characteristic length was adjusted to give different $\dot{S}_i$ and therefore Gr. It is important to consider the dependence of resolution of the mesh on Gr in the context of the above definition. The mesh is at its finest resolution for the lowest values of Gr and the resolution becomes coarser, as Gr is increased. The significance of such a modification to the geometry could have an impact on the state selected by the solver ANSYS CFX (ANSYS, 2007). The only way that the most stable state can be selected with ANSYS CFX (ANSYS, 2007) is via mesh refinement until no further changes in the state are observed. Thus, there is an inherent questionability on the physical representativeness of the circulation cells obtained in this study, particularly at the higher values of Gr.

The Prandtl number, $Pr = \nu / \alpha$, has been shown to have some influence on the critical limit of Gr that could be correlated over the range $0.1 < Pr < 35$ for inclined homogeneous heated flows between two isothermal planes (Generalis and Nagata, 2003; Gershuni, Zhukhovitsky and Yakimov, 1974). Thus, $Pr\ 7$ was selected to avoid a strong influence of the thermal diffusivity on the critical limit of Gr, where the product, $GrPr$, gives the Rayleigh number, Ra, another measure of the stability of cellular convective flows.

2.4 Solution convergence

The selected advection scheme was the high-resolution scheme, with trilinear interpolation of the velocity and pressure fields. The Boussinesq approximation, the fifth term in Eq. (2), was applied via the buoyant flow model with a reference temperature. All the calculations have been performed in the steady state mode. Nevertheless, the time remains in Eqs. (2) and (3), as it is reliant on the definition of the "characteristic time". The solver ANSYS CFX (ANSYS, 2007) uses a pseudo-steady state model, where time controls the speed at which the solution is progressed. This time scale acts as an extra level of under-relaxation, which was defined as $L^2/4\nu$. Further under-relaxation factors can be modified elsewhere in the solver, however these factors were left at their default values. The solutions that are presented here all attained a steady state where the velocity components are time invariant. For most of the cases presented here, this steady state was only achieved at residual errors of less than 10^{-8}.

3. RESULTS AND DISCUSSION

For the case of an internally heated layer that had an isothermal plane above an adiabatic plane, $\varepsilon = (Gr - Gr_c)/Gr_c$ was increased from -0.42 to 17. For the selected fluid and conditions, $Gr_c = 197.71$, or for the critical value of *Ra*, which was reported as $Ra_c = 1386$ by Ichikawa et al. (2006). The resultant solutions for the convection initially take the form of a laminar layer, which is then disturbed by the circulation cells that are formed when $\varepsilon > 0$ as indicated by the change in characteristic parameters plotted in Fig. 2 to Fig. 5. Fig. 2 presents the non-dimensionalised temperature difference and the increase in the approximate circulation cell size is given in Fig. 3, whilst Fig. 4 illustrates the variation the non-dimensionalised velocity components and the first six Fourier space modes are depicted in Fig. 5. Contours of the temperature and velocity fields are also given in Fig. 6 and Fig. 7 along with Table 1 detailing the wavenumber of the circulation cells.

3.1 Convection phenomena

The stable structures are formed in the following sequence: longitudinal rolls then squares, hexagons, pentagons and again squares; however, the squares have different orientations as depicted in Fig. 6 and Fig. 7. Note that when $\varepsilon >> 17$ the heated layer becomes unstable, which corresponds to the range of ε for stable hexagonal circulation cells, as reported by Tveitereid and Palm (1976) for the case of internally heated convection in a similarly bounded horizontal layer. This is despite the formation of several different patterns in the current study, which were also indicated in the analysis of Roberts (1967).

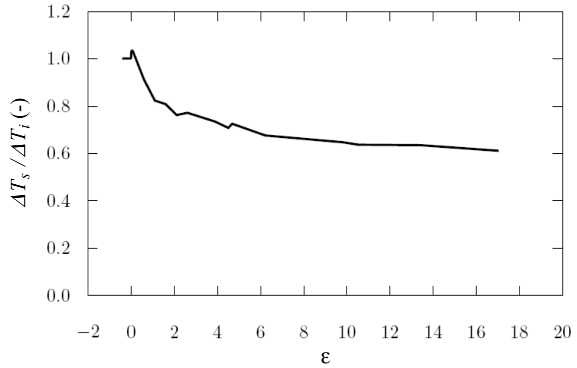

Fig. 2 Profiles of the non-dimensionalised temperature difference as the value of ε is increased.

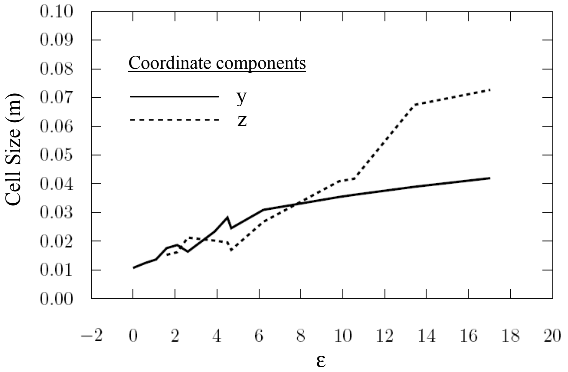

Fig. 3 Profiles of the circulation cell size as the value of ε is increased.

The evolution of the temperature (Fig. 2) has a peak at $\varepsilon = 0$, which is then followed by an asymptotic decrease as ε is increased. The temperature difference is consistent with those reported by Ichikawa et al. (2006) at $\varepsilon \approx 2.6$. Note that the heat flux through the upper isothermal boundary was up to about -300 W/m^2, which may be the cause of the deviation in the temperature difference from the laminar state observed in Fig. 2. At the same time that there is a change in the temperature profile, the sizes of the various circulation cells that are formed are indicated in Fig. 3. The cells increase in size as ε is augmented and are comparatively stretched along the z-axis when $\varepsilon >> 6$. Note that at $\varepsilon = 3.9$ and 4.7, the value of *Pr* was slightly less than the specified value of 7. This had no significant impact on the temperature, cell sizes, velocity components or the Fourier modes as ε is augmented in the profiles observed in Fig. 2 to Fig. 5. In particular, the resolved flow field at $\varepsilon = 4.5$ gave the same distribution of the circulation cells as those observed at $\varepsilon = 4.7$, where the distribution can be seen in the temperature and *u* velocity component contours presented in Fig. 6h and Fig. 7h.

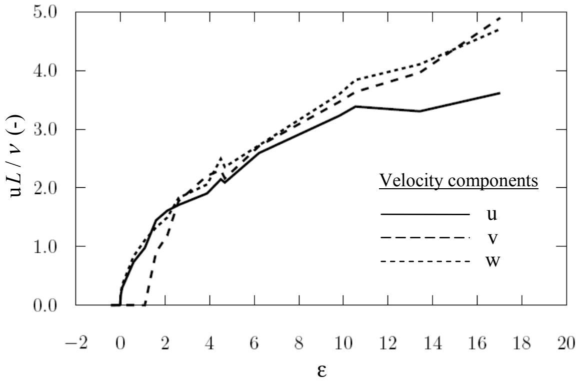

Fig. 4 Profiles of the non-dimensionalised velocity components as the value of ε is increased.

The velocity components depicted in Fig. 4 display a significant increase in the *u* and *v* velocity components at $\varepsilon = 0$; however the *w* velocity component does not increase until $\varepsilon > 1.1$ and again at $\varepsilon > 2$. The increases in velocity are respectively associated with changes in the state of the fluid layer (see also Fig. 6 and Fig. 7), from z-axis rolls to squares to what could be considered isotropic hexagons (Groh et al., 2007). However, Groh et al. (2007) stated that hexagons are isotropic in two dimensions, which is not the case in this study as the hexagons are isotropic with regards to the magnitude of three velocity components. The velocities become anisotropic at values of $\varepsilon >> 6$ as the velocities lose their similarity and there is a concurrent change in the flow state, as the circulation cells expand.

3.2 Fourier analysis

A Fourier analysis of *u* velocities that were estimated on the midlayer plane (Fig. 1) was performed using Fast Fourier Transform of Frigo and Johnson (2005) that is available to use in the Octave numerical language (Eaton, Bateman and Hauberg, 2007). This enabled the identification of the significant modes that categorise the different states. The relative amplitudes, ℓ^2, of the first six Fourier space modes are found to vary with ε, which are plotted in Fig. 5.

Fourier space modes have long been used in the description and prediction of the formation of rolls, hexagons and squares in various forms of thermal convection. The technique, first introduced by Busse (1967), was applied recently in the analysis of rolls and hexagonal cells in an experimental study of convection in a so-called *ferrofluid* that was driven by two magnetic fields at right angles to one another (Groh et al., 2007). A new saddle node bifurcation was identified by Groh et al. (2007), as a result of their analysis that bridges hexagons and stripes.

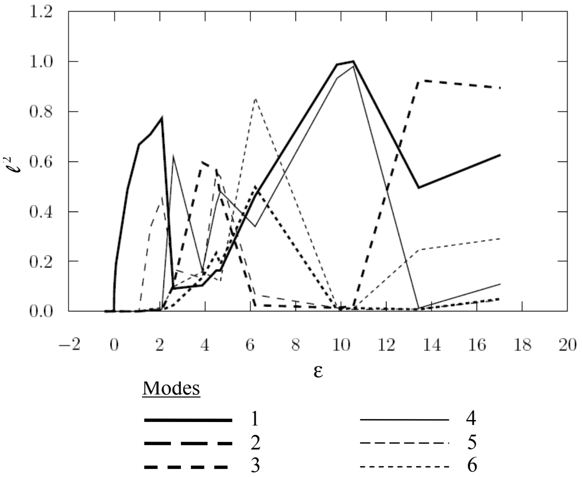

Fig. 5 Profiles of the relative amplitude of the first six modes in Fourier space as the value of ε is increased.

The first mode (Fig. 5) is associated with the z-axis rolls (see Fig. 6b to Fig. 6e and Fig. 7b to Fig. 7e) that are observed in the range $0 < \varepsilon < 1$ with an increase in its amplitude. Note that ℓ^2 is the amplitude relative to the maximum amplitude of all the observed frequencies. For the first of three square circulation cell states (Fig. 6f & Fig. 7f), ℓ^2 of the sixth mode is also significant (Fig. 5); thus according to linear theory this state should be associated with waves in the spanwise direction.

The next states are observed at $\varepsilon = 2.6$ where all of the six modes show some effect on the horizontal layer (Fig. 5). Examining both the temperature (Fig. 6g & Fig. 6h) and *u* velocities (Fig. 7g & Fig. 7h), hexagonal and several pentagonal circulation cells are observed. At $\varepsilon = 2.6$, the first, third and fifth modes depicted in Fig. 5 all have a similar ℓ^2 whilst the second and sixth modes are within ± 0.08 of this amplitude and the fourth mode is quite different. However, at $\varepsilon = 3.9$, all the modes have an ℓ^2 of 0.13 ± 0.03 except for the third mode. At $\varepsilon = 4.5$ and 4.7, the modes are arranged into two groups with relative amplitudes of 0.17 ± 0.06 for the first, second and fifth modes and at 0.50 ± 0.07 for the remaining modes.

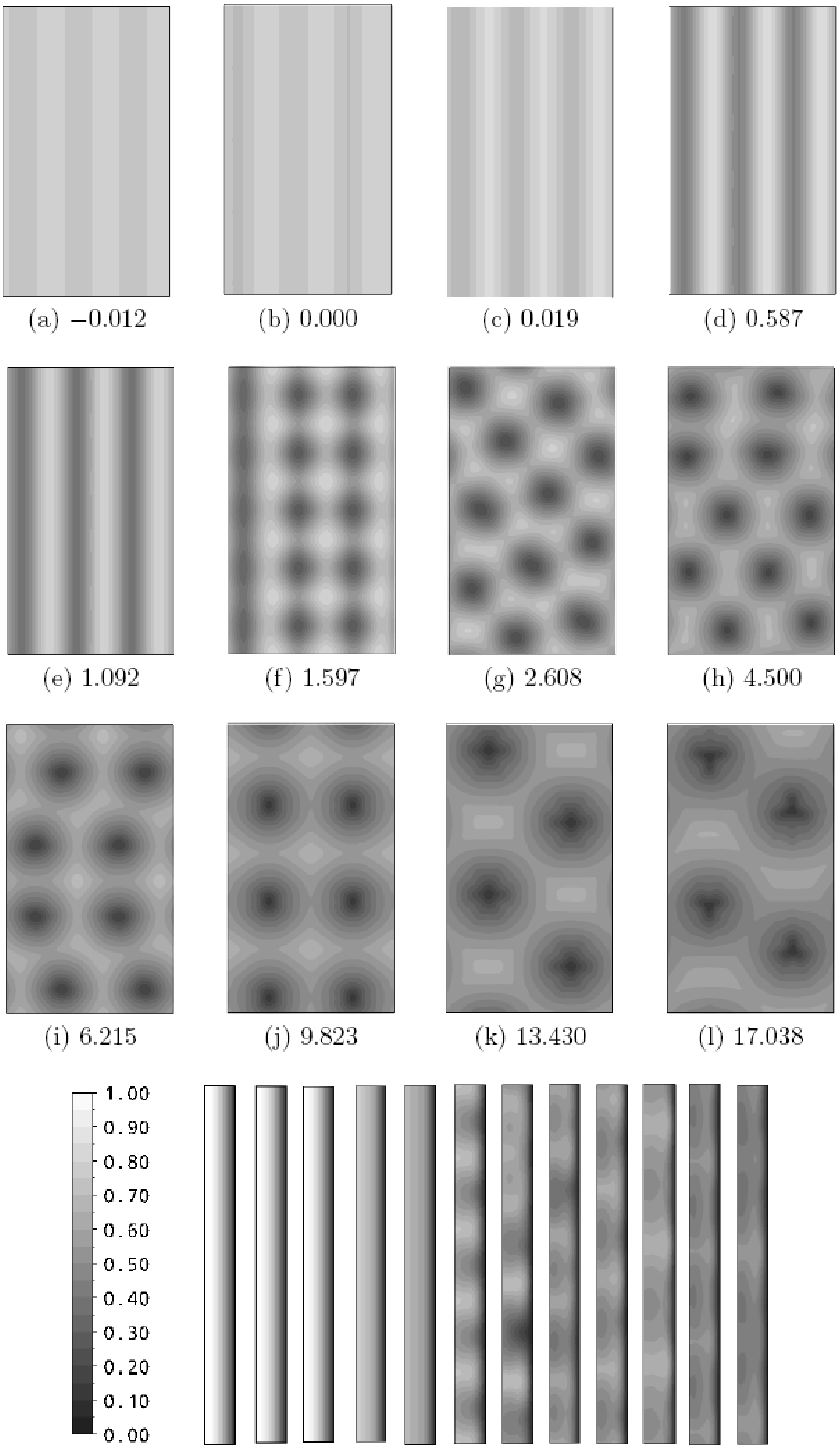

(a) −0.012 (b) 0.000 (c) 0.019 (d) 0.587

(e) 1.092 (f) 1.597 (g) 2.608 (h) 4.500

(i) 6.215 (j) 9.823 (k) 13.430 (l) 17.038

(m) $\epsilon = -0.012 \longrightarrow 17.042$

Fig. 6 Temperature contours on the midlayer and the corresponding spanwise planes in Fig. 1 for increasing values of ε.

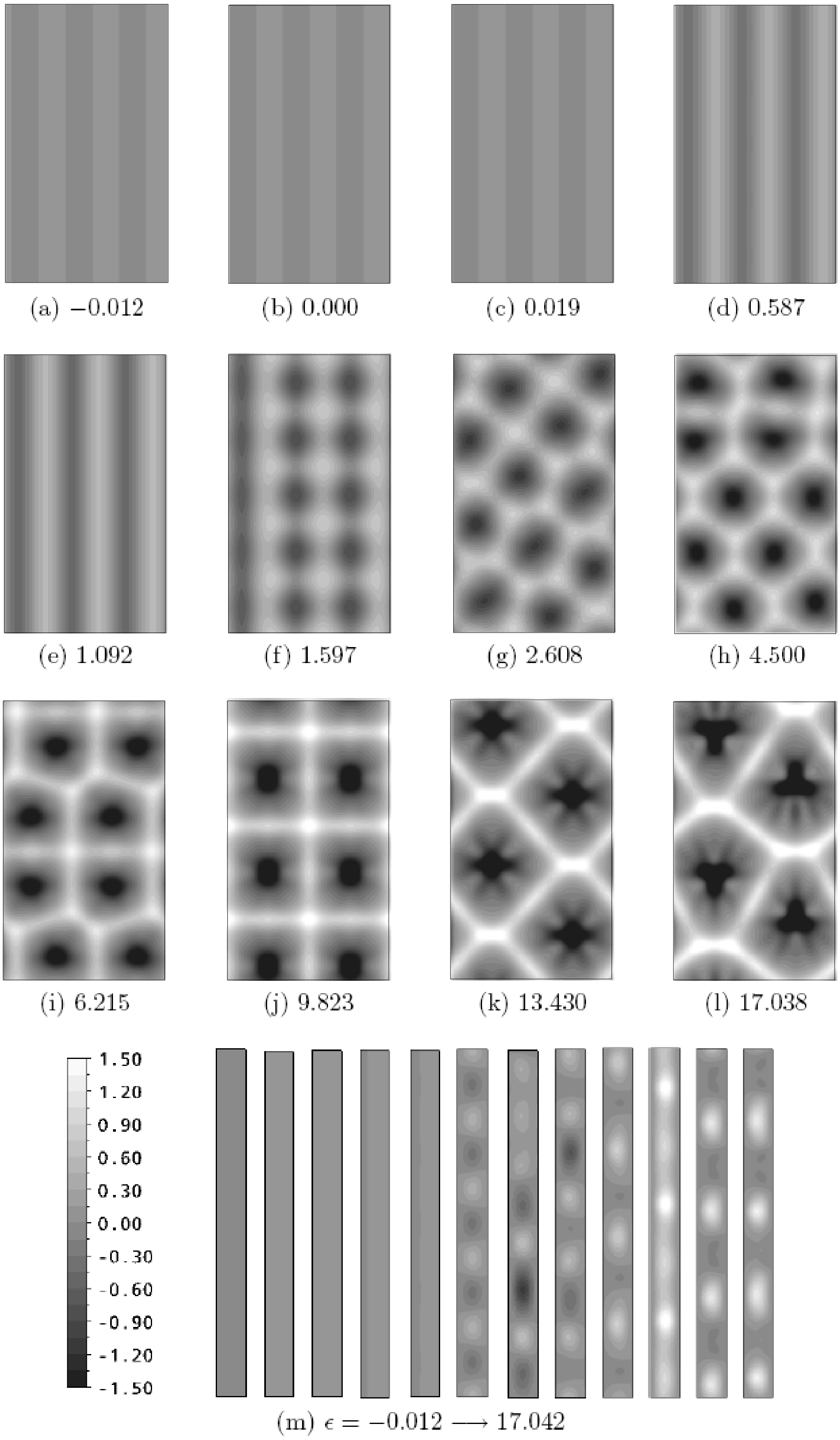

(a) −0.012 (b) 0.000 (c) 0.019 (d) 0.587

(e) 1.092 (f) 1.597 (g) 2.608 (h) 4.500

(i) 6.215 (j) 9.823 (k) 13.430 (l) 17.038

(m) $\epsilon = -0.012 \longrightarrow 17.042$

Fig. 7 *u* velocity component contours on the midlayer and the corresponding spanwise planes in Fig. 1 for increasing values of ε.

At $\varepsilon = 6.2$, there is a spread of the modes, where what seems to be distorted pentagons (Fig. 6i & Fig. 7i) are the only circulation cells present. At this point, ℓ^2 for the third and sixth modes become insignificant when compared to the other four modes (Fig. 5).

At $\varepsilon = 10$, a second square state is formed (Fig. 6j & Fig. 7j), but this state varies in orientation from the earlier square state. The modes that characterise the behaviour of both square states also differ, as modes 1 and 4 characterise the second square state rather than modes 1 and 6 of the first square state (Fig. 5). A third square state is formed at $\varepsilon > 13$ (Fig. 6k & Fig. 6l with Fig. 7k & Fig. 7l), where again the orientation of the cells is changed and the significant modes in Fig. 5 are the first and third modes whilst the fourth and sixth modes are insignificant. However, in this case spokes are formed within the circulation cell. As ε is increased towards the transient regime, the square circulation cell is stretched along the z-axis, which can be associated with either the first or the fifth mode (Fig. 5).

3.3 Wavenumber analysis

In order to further emphasize the change in the cellular flow with increased ε, the wavenumber, $\vec{k} = 2\pi L/\lambda$, was estimated with the wavelength λ as either the distance between minima in the *y* or *z* component direction or in the form of radii, *r*. The values of $\vec{k}$ presented in Table 1 were determined from the distance between the temperature minima of the six nearest neighbours and the temperature minima of the circulation cell closest to the centre of the modelled domain. Note that the minima for the laminar layers and the longitudinal rolls were not sorted with regards to the distance from the central minima (i.e. cases over the range $-0.423 < \varepsilon < 1.092$). For cases K and L, the $\vec{k}$ values were also not sorted, due to the small number of minima.

The values of $\vec{k}$ (Table 1) show no order for the laminar layers in the range $-0.423 < \varepsilon < -0.012$, while the values of the y component of $\vec{k}$ are constant for all of the minima between $\varepsilon = 0.000$ and 1.092. The $\vec{k}$ value also shows the effect of the *z* component even though this has no bearing on the behaviour of the rolls as the selected minima were obtained from the same roll in each case.

For the squares observed with $\varepsilon = 1.597$ and 2.102 (Table 1), the first four values depend on minima that are aligned on the *y* or *z* axis with respect to the central minima. Minima five and six for both these cases correspond to points that are adjacent to the central minima; however, these locations are a little further away from the *y* and *z* axis aligned minima. Note that these points are positioned at a 45° angle to either *y* or *z* axis.

Table 1 indicates that the $\vec{k}$ values of the circulation cells are between 0.9 and 1.3 in the range $2.608 < \varepsilon < 4.681$. These values correspond to the *r* component direction and suggest that the circulation cells are hexagonal due to their similarity. At $\varepsilon = 6.215$, the corresponding $\vec{k}$ values are slightly larger with values between 0.8 and 1.4. In this case, pentagonal structures were the circulation cells that were resolved. From the data available with the *y* and *z* direction dependent components of $\vec{k}$, the alignment of the hexagons and pentagons cannot directly be defined from the $\vec{k}$ values.

The square circulation cells of case J and V $(\varepsilon \in 9.823, 10.544)$ that were described earlier show their alignment with the infinite values of $\vec{k}$ defined with respect to y and z axes (Table 1). The minima where only finite $\vec{k}$ values are found correspond to circulation cells at 45° to both the y and *z* axes.

The orientation of the squares changes for a third time, as previously mentioned with cases K and L $(\varepsilon \in 13.430, 17.038)$. Due to the presence of only four full circulation cells in both cases K and L, the $\vec{k}$ values in Table 1 were left unsorted. Thus, $\vec{k}$ values 1–3 correspond to the full circulation cells and values 4–6 correspond to cells that cross the periodic boundaries. Note that the $\vec{k}$ values in the *y* direction are similar for the full circulation cells and the infinite value corresponds to a circulation cell that is in line with the first of the four minima. The $\vec{k}$ values calculated for both cases K and L with respect to the *z* axis show a similar tendency to one another. Note that the key difference of the square circulation cells over the range $9.823 < \varepsilon < 17.038$ is that the cells for cases J and V have a 90° pitch, whereas the cells for cases K and L were arranged in a 45° pitch.

Table 1 Wavenumber calculated with respect to distance of the first six adjacent circulation cells, where cases A to L correspond to the cases depicted in Fig. 6 and Fig. 7.

Case	ε		$\vec{k}$					
			1	2	3	4	5	6
M	-0.423	r	0.60	0.44	1.37	0.64	0.58	0.45
		y	2.22	2.33	-1.50	0.65	-1.50	0.65
		z	-0.62	0.45	3.35	3.35	-0.62.	-0.62
N	-0.170	r	0.32	0.46	0.81	0.61	0.58	0.62
		y	-1.41	-0.55	2.59	-0.65	-0.64	-0.69
		z	0.32	0.84	0.85	1.74	-1.38	-1.42
O	-0.044	r	1.37	0.52	11.66	0.78	0.51	0.53
		y	-2.59	0.55	-11.66	-15.55	0.66	0.69
		z	1.62	1.62	∞	-0.78	-0.79	-0.82
A	-0.012	r	0.50	0.48	2.12	2.10	0.53	0.51
		y	1.41	1.41	-2.12	-2.12	11.66	11.66
		z	-0.53	0.51	46.86	15.62	-0.53	0.51
B	0.000	r	0.42	0.41	0.43	0.43	0.45	0.60
		y	0.69	0.69	0.69	0.69	0.69	0.69
		z	-0.53	0.51	-0.54	-0.56	-0.59	-1.27
P	0.001	r	0.41	0.43	0.41	0.44	0.44	0.46
		y	0.69	0.69	0.69	0.69	0.68	0.69
		z	-0.50	0.54	-0.52	-0.56	-0.59	-0.61
C	0.019	r	0.47	0.62	0.42	0.43	0.44	0.45
		y	0.68	0.68	0.68	0.68	0.68	0.68
		z	-0.64	-1.51	-0.54	-0.56	-0.58	-0.61
Q	0.051	r	0.38	0.40	0.69	1.14	0.68	0.66
		y	1.33	1.33	1.33	1.33	1.33	1.33
		z	-0.40	-0.42	-0.81	2.23	0.79	0.76
R	0.082	r	0.58	0.42	0.62	0.64	1.09	1.14
		y	1.33	1.33	1.33	1.33	1.33	1.33
		z	-0.64	0.44	-0.70	-0.73	-1.87	-2.23
D	0.587	r	0.46	0.47	0.49	0.48	0.52	0.54
		y	0.69	0.69	0.69	0.69	0.69	0.69
		z	-0.62	-0.63	-0.71	-0.67	-0.81	-0.88
E	1.092	r	0.41	0.43	0.44	0.46	0.47	0.60
		y	0.69	0.69	0.69	0.69	0.69	0.69
		z	-0.50	0.54	-0.58	-0.62	-0.65	-1.27
F	1.597	r	1.37	1.37	1.30	1.30	0.94	0.94
		y	-1.37	1.37	∞	∞	-1.37	1.37
		z	∞	∞	-1.30	1.30	-1.30	-1.30
S	2.102	r	1.41	1.33	1.30	1.30	0.96	0.96
		y	-1.41	1.33	∞	∞	-1.41	-1.41
		z	∞	∞	-1.30	1.30	-1.30	1.30
G	2.608	r	1.19	1.14.	1.11	1.11	1.02	0.82
		y	1.46	1.67	-1.79	-1.14	-5.18	6.66
		z	2.04	-1.56	1.42	-4.69	-1.04	0.82
T	3.886	r	1.12	1.10	1.03	1.02	0.95	0.87
		y	1.20	2.22	-2.12	1.20	-1.01	2.12
		z	3.12	-1.27	1.17	-1.95	-2.76	0.96

Table 1 (Continued)

Case	ε		$\vec{k}$					
			1	2	3	4	5	6
		r	1.26	1.08	1.07	1.05	1.05	0.91
H	4.500	y	1.26	1.94	1.87	-1.79	-1.87	-0.91
		z	-46.86	-1.30	1.30	-1.30	1.27	-46.86
		r	1.23	1.12	1.10	1.08	1.03	0.91
U	4.681	y	1.23	1.94	2.03	-1.73	-1.67	-0.91
		z	46.86	-1.38	1.30	-1.38	1.30	46.86
		r	1.37	1.04	0.98	0.91	0.84	0.83
I	6.215	y	-1.37	∞	-2.91	0.91	-1.37	1.33
		z	-23.43	-1.04	1.04	∞	-1.07	1.07
		r	0.91	0.79	0.78	0.60	0.59	0.43
J	9.823	y	0.91	∞	∞	0.91	0.91	∞
		z	∞	-0.79	0.78	-0.79	0.78	0.43
		r	1.33	0.91	0.79	0.78	0.68	0.67
V	10.544	y	-1.33	0.91	∞	∞	-1.33	-1.33
		z	∞	∞	-0.79	0.78	-0.79	0.78
		r	0.33	0.69	0.53	0.29	0.29	0.61
K	13.430	y	-0.91	-0.91	∞	-11.66	11.66	-0.61
		z	-0.35	-1.04	-0.53	-0.29	-0.29	∞
		r	0.80	0.36	0.54	0.73	0.60	1.35
L	17.038	y	0.91	0.91	∞	0.91	0.61	-1.79
		z	1.67	0.39	0.54	-1.20	9.37	2.04

4. CONCLUDING REMARKS

The main motivation of this work was to examine thermal convection that is produced by a homogeneous heat source. The boundary conditions that we adopted were that the bottom boundary was an adiabatic plane while the upper boundary was an isothermal plane. Our study concentrated exclusively on the interplay of the cells that bifurcate as a control parameter varies. In the process of our studies we attempted to make contact with previous work and benchmark our results against available data in the literature. We used Fourier and wavenumber analyses in order to be able to identify the leading modes that categorize the different cells that compete. Hysteresis effects were also examined and it was shown that in the case considered here polygonal structures are the predominant form of cells for a wide range of the control parameter. We note that both Groh et al. (2007) and Thiele and Eckert (1998) categorised the evolution of circulation cells from hexagons to other structures via two distinct methods. As previously mentioned Groh et al. (2007) examined the Fourier space modes whilst Thiele and Eckert (1998) used a stochastic geometrical method to identify the different structures. However, in the case of Groh et al. (2007) only rolls were formed from the stretching of the hexagons as magnetic fields were altered. Hexagonal flip to roll structure was substantiated there via a Stuart-Landau equation. Thiele and Eckert (1998) showed that both hexagons and pentagons could coexist in a *Bénard-Marangoni* layer via analysis of the vertices of the circulations cells. It was also shown that the state could change from hexagonal cells to pentagons then to squares through the loss of one or two of these vertices. These vertices could be considered equivalent to the Fourier space modes, which have been used here to identify or categorise the different circulation cells predicted by the simulations performed here. However, in the case of Thiele and Eckert (1998) the patterns were initially hexagonal before reduction in the significance of one or two of the vertices occurred, whilst in the current study the initial patterns were z-axis rolls followed by squares, then hexagons and pentagons and then back to squares as the importance of the different modes changed with the increase in *ε*.

Hexagonal cells are the preferred mode for the evolution of instabilities in homogeneous systems. However, for cases where the breaking of isotropy is insignificant, rolls seem to be the preferred mode of evolution. Yet when isotropy is broken by the temperature dependence of material properties such as viscosity (Busse, 1967) then the stability of the rolls is reduced, as the magnitude of the isotropic breaking term increases.

The cases described here, considered an additional heat flux that was applied homogeneously to a fluid layer with asymmetric boundary conditions. The study showed that the preferred mode of instability is hexagons for fluids with Prandtl numbers of O(10). Further investigations are being performed to identify the stability characteristics as a function of the Grashof and wavenumbers. In addition, the instability of internally heated layers of fixed depth with rigid, conducting or insulating boundaries have also been examined along with the effect that a pressure gradient has on the generated circulation cells (Generalis and Busse, 2008).

ACKNOWLEDGEMENTS

We wish to thank the Institute for Safety Research at the Forschungszentrum Dresden-Rossendorf for kindly allowing access to the computational cluster upon which the calculations were performed.

NOMENCLATURE

c_p	specific heat capacity at constant pressure, J/(kg K)
e	internal energy, J/kg
Gr	Grashof number $Gr = \vec{g}\,\beta\,\dot{S}_i\,L^5 \big/ 2\,v^2\,k$
Gr_c	critical Grashof number $Gr_c = 198$
$\vec{g}$	acceleration due to gravity, m/s^2
$\vec{k}$	Wavenumber
k	thermal conductivity, W/(m K)
L	characteristic length, m
ℓ^2	relative amplitude of the Fourier modes (-)
Pr	Prandtl number $Pr = v \,/\, \alpha = 7$
p	pressure, kg/(m s^2)
Ra	Rayleigh number $Ra = GrPr$
Ra_c	critical Rayleigh number $Gr_c = 1386$
r	radius between circulation cell minima, m
$\vec{S}$	momentum source terms, kg/(m^2 s^2)
$\dot{S}$	energy source terms, kg/(m s^3)
$\dot{S}_i$	internal heat source, kg/(m s^3)
T	temperature, K
T_r	reference temperature, K
ΔT_i	temperature difference due to internal heating, 1 K
ΔT_s	temperature difference of the solved flow, K
t	time, s
$\vec{u}$	velocity vector {u, v, w}, m/s
$\vec{x}$	position vector {x, y, z}, m
$\vec{x}_c$	position vector of the temperature minima of the central circulation cell, m
$\vec{x}_i$	position vector of the temperature minima of the ith circulation cell, m

Greek Symbols

α	thermal diffusivity, m^2/s
β	expansion coefficient, 1/K
ε	reduced Grashof number, $\varepsilon = \left(\ Gr - Gr_c\ \right) / \ Gr_c$
λ	wavelength, m, $\lambda = \vec{x}_i - \vec{x}_c$
μ	dynamic viscosity, kg/(m s)
v	kinematic viscosity, m^2/s
ρ_r	reference density, kg/m^3

REFERENCES

1. ANSYS (2007). *ANSYS CFX 11*. ANSYS Inc., Canonsburg, PA, USA.
2. Arter W, Bernoff A, Newell AC (1987). Wavenumber selection of convection rolls in a box. *Physics Fluids* 12(12):3840–3842.
3. Asfia FJ, Dhir VK (1996). An experimental study of natural convection in a volumetrically heated spherical pool bounded on top with a rigid wall. *Nuclear Engineering Design* 163:333–348.
4. Busse FH (1967). The stability of finite amplitude cellular convection and its relation to an extremum principle. *J. Fluid Mechanics* 30(4):625–649.
5. Eaton JW, Bateman D, Hauberg S (2007). *GNU Octave: A high-level interactive language for numerical computations*. Octave.org. University of Wisconsin, Madison, WI, USA.
6. Frigo M, Johnson SG (2005). The design and implementation of fftw3. *Proceedings of the IEEE* 93:216–231.
7. Generalis S, Nagata M (2003). Transition in homogeneously heated inclined plane parallel shear flows. *J. Heat Transfer* 125:795–803.
8. Generalis SC, Busse FH (2008). Transition in inclined internally heated fluid layers.

Proceedings of the 5th European Thermal-Sciences Conference, no. FCV 10, Eindhoven, 2008.

9. Gershuni GZ, Zhukhovitsky EM, Yakimov AA (1974). On stability of plane-parallel convective motion due to internal heat sources. *Int. J. Heat Mass Transfer* 17(7):717–726.
10. Groh C, Richter R, Rehberg I, Busse FH (2007). Reorientation of a hexagonal pattern under broken symmetry: The hexagon flip. *Physical Review E* 76:055301(R).
11. Houseman G (1988). The dependence of convection planform on mode of heating. *Nature* 332:346–349.
12. Ichikawa H, Kurita K, Yamagishi Y, Yanagisawa T (2006). Cell pattern of thermal convection induced by internal heating. *Physics Fluids* 18:038101.
13. Roberts PH (1967). Convection in horizontal layers with internal heat generation. Theory. *J. Fluid Mechanics* 30(1):33–49.
14. Schmalzl J, Houseman GA, Hansen U (1995). Mixing properties of three-dimensional (3-d) stationary convection. *Physics Fluids* 7(5):1027–1033.
15. Schubert G, Glatzmaier GA, Travis B (1993). Steady, three-dimensional, internally heated convection. *Physics Fluids* 5(8):1928–1932.
16. Thiele U, Eckert K (1998). Stochastic geometry of polygonal networks: An alternative approach to the hexagon-square transition in Bénard convection. *Physical Review E* 58(3):3458–3468.
17. Tritton DJ, Zarraga MN (1967). Convection in horizontal layers with internal heat generation. *J. Fluid Mechanics* 30(1):21–31.
18. Tveitereid M, Palm E (1976). Convection due to internal heat sources. *J. Fluid Mechanics* 76:481–499.